ACI MATERIALS JOURNAL TECHNICAL PAPER

Title No. 114-M69

Complete Stress-Strain Behavior of Ecological Ultra-High-Performance Cementitious Composite under Uniaxial Compression

by Zhiyong Liu, Weiwei Chen, Wenhua Zhang, Yunsheng Zhang, and Henglin Lv

An ecological ultra-high-performance cementitious composite (ECO-UHPCC) was investigated in this paper. The ECO-UHPCC has three characteristics: low cement content (400 to 520 kg/m³ [24.97 to 32.46 lb/ft³]), contains nature river sand and high-strength coarse aggregate, and is cured in standard condition. The complete stress-strain behavior of ECO-UHPCC under uniaxial compression was systematically investigated. First, a series of ECO-UHPCC specimens containing different coarse aggregates and steel fibers were fabricated. Second, the uniaxial compressive tests were conducted by a high-stiffness, closed-loop, servo-controlled, material testing machine, and the complete stress-strain curves of ECO-UHPCC were obtained. Then, the results, including complete stress-strain behavior, compressive strength, elastic modulus, Poisson's ratio, toughness, and fracture pattern of ECO-UHPCC were systematically analyzed. The test results show that ECO-UHPCC exhibits better compressive strength and stiffness than high-performance concrete. The compressive strength and elastic modulus of ECO-UHPCC with basalt coarse aggregate and 2% steel fiber were up to 128.4 MPa (18.62 ksi) and 46.2 GPa (6700.51 ksi), respectively. Finally, a new model was developed for predicting the complete stress-strain behavior of ECO-UHPCC under uniaxial compression. This model shows a good correlation with the experimental results.

Keywords: ecological ultra-high-performance cementitious composite (ECO-UHPCC); model; stress-strain behavior; uniaxial compression.

INTRODUCTION

Ultra-high-performance cementitious composite (UHPCC) is an advanced cement based material[1,2] that has exceptional compressive and flexural strength, superior ductility, and excellent durability.[3-5] It has a great potential for use in high-rise buildings, large-span space structures, bridge engineering, and military engineering.[6,7]

To obtain superior mechanical properties, UHPCC is composed of a high dosage of cement (generally 900 to 1000 kg/m³ [56.18 to 62.42 lb/ft³]), very fine powder (such as crushed quartzite and silica fume), and steel fiber.[1] Obviously, these expensive raw materials are responsible for high energy consumption, which results in significant emissions of greenhouse gases.[8] In addition, the rigorous curing regimes of 200°C (392°F) autoclave curing or 90°C (194°F) heating curing are usually employed in the fabrication of UHPCC,[1,9-11] which results in very high energy consumption and restricts this advanced material being used for cast-on-site engineering. Moreover, for the enhancement homogeneity, the coarse aggregates are eliminated in UHPCC.[1] The elimination of the coarse aggregate means the much higher amount of cementitious material dosage. This leads to a sharp increase in autogenous shrinkage and rapid surface drying that form premature shrinkage cracks of the UHPCC,[12-15] which may reduce its early-age and hardened performance. Therefore, reducing production cost and energy consumption, simplifying the manufacturing process, and eliminating the negative effectives caused by the high amount of cementitious dosage are the key challenges for the application of UHPCC in practical engineering.

In this paper, an ecological ultra-high-performance cementitious composite (ECO-UHPCC) was fabricated by the following methods. First, a large amount of portland cement (≥50%) is replaced by industrial waste, including fly ash, slag, and silica fume. The cement content of ECO-UHPCC ranges from 400 to 520 kg/m³ (24.97 to 32.46 lb/ft³). Second, natural river sand with a maximum size of 3 mm (0.1182 in.) substitutes for the costly ultra-fine quartz sand. Third, the standard curing (20°C [68°F] and 100% RH) takes the place of rigorous curing regimes. Finally, high-strength coarse aggregates are used to reduce the cementitious material dosage. The ECO-UHPCC has an equivalent mechanical performance to UHPCC.

Understanding the response of ECO-UHPCC to compressive loading is important for successful analysis and design of structures. Many studies had been conducted on the mechanical properties of UHPCC.[2-5,16-21] Accordingly, Graybeal[21] conducted compressive tests to determine the overall stress-strain behavior of ultra-high-performance fiber-reinforced concrete (UHPFRC). However, because of the limitation of the test machine, the ascending part of the stress-strain curve was obtained without the descending part. Additionally, most of the other studies mainly concentrated on the cube or cylinder compressive strength of UHPCC.[2-5,16-20] Therefore, research devoted to investigating the complete stress-strain behavior of UHPCC in uniaxial compression is very limited.

The uniaxial compressive behaviors of the ECO-UHPCC were systematically investigated. First, the ECO-UHPCC specimens with different coarse aggregates and steel fibers were fabricated. Second, the uniaxial compressive tests on ECO-UHPCC were conducted by a special closed-loop, servo-controlled, material testing machine. Third, the complete stress-strain behaviors of ECO-UHPCC, including compressive strength, elastic modulus, Poisson's

ACI Materials Journal, V. 114, No. 5, September-October 2017.

MS No. M-2016-350.R2, doi: 10.14359/51689899, received November 4, 2016, and reviewed under Institute publication policies.

Table 1—Mixture proportions, kg/m³

	Mixture No.	Water	Cement	Silica fume	Fly ash	Slag	Sand	Coarse aggregate	Steel fiber	HRWRA	Maximum size of aggregate, mm
Control mixture	CM	164	512	102.4	204.8	204.8	1024	0	0	25.6	—
Aggregate size (AS)	AS-10	128	400	80	160	160	800	800	0	20	10
	AS-15	128	400	80	160	160	800	800	0	20	15
	AS-20	128	400	80	160	160	800	800	0	20	20
Aggregate type (AT)	AT-G	128	400	80	160	160	800	728	0	20	10
	AT-B	128	400	80	160	160	800	800	0	20	10
	AT-I	128	400	80	160	160	800	1335	0	20	10
Steel fiber content (FC)	FC-1	164	512	102.4	204.8	204.8	1024	0	78	25.6	—
	FC-2	164	512	102.4	204.8	204.8	1024	0	156	25.6	—
	FC-3	164	512	102.4	204.8	204.8	1024	0	234	25.6	—
	FC-4	164	512	102.4	204.8	204.8	1024	0	312	25.6	—
	FC-5	164	512	102.4	204.8	204.8	1024	0	390	25.6	—
Steel fiber type (FT)	FT-S	164	512	102.4	204.8	204.8	1024	0	156	25.6	—
	FT-D	164	512	102.4	204.8	204.8	1024	0	156	25.6	—
	FT-H	164	512	102.4	204.8	204.8	1024	0	156	25.6	—
Optimized mixture	OM	128	400	80	160	160	800	800	156	20	10

Notes: 1 kg/m³ = 0.0624 lb/ft³; 1 mm = 0.0394 in.

ratio, toughness, and fracture pattern, were systematically discussed. Finally, a new model was developed for predicting the complete stress-strain behavior of ECO-UHPCC.

RESEARCH SIGNIFICANCE

The complete stress-strain relationships of ECO-UHPCC under uniaxial compression were systematically investigated. The results, including complete stress-strain behavior, compressive strength, elastic modulus, Poisson's ratio, toughness, and fracture pattern of ECO-UHPCC, were analyzed. An analytical model was developed for predicting the complete stress-strain behavior of ECO-UHPCC under uniaxial compression.

MATERIALS AND METHODS

Raw materials

Four types of cementitious materials were used in this study: portland cement (PC) with a 28-day compressive strength of 68.9 MPa (9.99 ksi), silica fume (SF), fly ash (FA), and slag (SL). Natural river sand with the maximum size of 3 mm (0.118 in.) was used to replace the ultra-fine quartz sand, which is a necessary component of UHPCC reported by published literature.[6,22] Three different types of coarse aggregate (CA) were used: crushed basalt, crushed granitic, and crushed iron ore. These aggregates were selected because they present significant differences in strength, surface texture, porosity and absorption, and bond strength. The crushed basalt has an irregular shape and rough texture. The crushed granitic presents irregular shape, rough texture, and low absorption. The crushed iron ore has a rough surface texture and the highest density. The same particle size distribution was adopted with a maximum aggregate size of 10 mm (0.394 in.). The grading of coarse aggregates satisfied the requirements of ASTM C33/C33M.[23] Density, porosity, and water absorption ratio index of the coarse aggregate were tested according to ASTM C127.[24] The compressive strength of the coarse aggregate was tested according to GB/T14685-200[25] of China. The test samples were cylinders with a size of ϕ50 x 50 mm (1.97 x 1.97 in.).

Three different steel fibers, including straight smooth steel fiber, hooked-end steel fiber, and dumbbell-shaped steel fiber, were used in this study. These steel fibers have different diameters and lengths, but the same aspect ratio (l/d) of 70.

Mixture design

First, an ECO-UHPCC control mixture (CM) was designed for comparing with the ECO-UHPCC containing different coarse aggregates and steel fibers. The water-binder ratio and sand-binder ratio of the mixture were 0.16 and 1.0, respectively. For cementitious binder, 50% of portland cement was replaced by ternary mineral admixtures composited of 10% silica fume, 20% fly ash, and 20% slag. A polycarboxylic type high-range water-reducing admixture (HRWRA) with water-reducing ratio of 40% was adopted to control workability. The dosage of HRWRA was kept at 2.5% weight of total binder. The mixture proportions of the CM are shown in Table 1.

Secondly, the AS-series and AT-series were designed based on CM. The AS-series were used to study the effect of aggregate size on the influence of mechanical properties. AS-10, AS-15, and AS-20 present the mixture containing coarse aggregate with the maximum size of 10, 15, and 20 mm (0.394, 0.591, and 0.787 in.), respectively. The AT-series was designed to investigate the aggregate type. AT-G, AT-B, and AT-I present that the ECO-UHPCC contains granitic, basalt, and iron ore coarse aggregate, respectively. The volume fraction of coarse aggregate must remain a constant value

of 27.5%. Because the steel fiber has a significant enhancement on compressive strength of UHPCC,[3,5] the steel fiber was not used in these six mixtures to isolate the effect of coarse aggregate.

Third, the FC-series and FT-series were also designed based on CM. FC-1 to FC-5 were designed to investigate the influence of steel fiber content (FC-series) on the compression behavior of ECO-UHPCC. For these five mixtures, the straight smooth steel fibers with volume fractions of 1%, 2%, 3%, 4%, and 5% were used. The FT-S, FT-H, and FT-D were designed to study the effect of steel fiber type (FT) on compressive properties, which present the ECO-UHPCC containing straight smooth steel fiber, hooked-end steel fiber, and dumbbell-shaped steel fiber. The volume fraction of those three mixtures is 2%.

Finally, on the basis of investigating influence of coarse aggregate and steel fiber, an optimized mixture (OM) of ECO-UHPCC containing 2% steel fiber as well as the basalt coarse aggregate with maximum size of 10 mm (0.394 in.) was proposed. All the mixtures proportions are shown in Table 1.

Specimen preparation

The ECO-UHPCC was mixed by a 56 L (1.98 ft^3) laboratory pan mixer. First, the cementitious materials (portland cement, silica fume, fly ash, and slag) and river sand were put into the mixer and dry-mixed for 1 minute. Second, the mixture of water and HRWRA was added and mixed for 3 minutes. Third, the coarse aggregates were poured into cementitious mixture and mixed for another minute. Finally, the steel fiber was sprinkled slowly into mixture and mixed for another 3 minutes to make steel fiber homogenously distributed through the fresh mixture. Then, the fresh ECO-UHPCC mixture was cast into steel molds and compacted by a vibrating table. The specimens were made in a cylindrical shape with a diameter of 75 mm (2.953 in.) and height of 150 mm (5.906 in.), which satisfies the requirements of ASTM C192.[26] The specimens were demolded after 24 hours and then cured in the standard condition of 20°C (68°F) and 100% relative humidity (RH) until 56 days.

To obtain accurate test results, specimen ends must be kept smooth and parallel to each other. Therefore, all the cylinder specimens were grinded by a special grinding machine before the compressive tests. During the grinding, ECO-UHPCC specimen was sandwiched between parallel grinding heads first, then the engine was started. The specimen would be automatically grinded smooth, and the two ends were kept parallel.

Testing methods

A high-stiffness, closed-loop, servo-controlled, material testing machine was used to conduct the compressive test. It is well known that the longitudinal stiffness of the testing machine is an important factor in compressive strength testing, which influences the post-peak response.[27,28] The rigid frame of this machine can avoid explosive failures of specimens and obtain the full stress-strain curves of ECO-UHPCC.

According to ASTM C469,[29] the strain of the compressive test specimen was obtained by the device that consists of two rigid circular rings and two linear variable differential transformers (LVDTs) connected to a digital transducer. However, this method is only able to capture the stress-strain values up to the first crack strength of the specimens. It is unable to capture the specimen strain behavior of post-cracking because the contact points of the LVDTs were disturbed and resulted in erratic readings. In this paper, a test method proposed by Mansur et al.[28] was used to overcome the shortage of the conventional method. In this method, four strain gauges were fitted over the specimens. Two were used to measure axial strain and the other two were used to measure transverse strain in the elastic stage of the test. In addition, two hardened rigid platens were specially fabricated, and the two LVDTs were secured on it. The LVDTs were used to capture the post-cracking behavior of specimen. During the test, the ECO-UHPCC specimens were sandwiched between the two hardened rigid platens. The cylinder compression tests were conducted according to ASTM C39/C39M.[30] The loading rate was 0.001 mm/s (3.94×10^{-5} in./s). The tests results were continuously recorded together with the corresponding loads; the data acquisition system took four readings per second. Three specimens of each batch were tested.

To obtain the complete stress-strain curve of the ECO-UHPCC, a correction was made according to the method introduced by Mansur et al.[28] In this correction method, Δ_{tp} is defined as the deformation measured by transducers placed between the top and bottom platens, Δ_{tp} is the deformation measured by strain gauge over a gauge length L_g, Δ_m is the deformation due to flexibility of the machine, Δ_e is the deformation due to end-zone effect, and Δ_c is the actual axial deformation of the specimen. It follows that

$$\Delta_{tp} = \Delta_c + \Delta_a \tag{1}$$

where $\Delta_a = \Delta_m + \Delta_e$.

Rearranging Eq. (1), and assuming that Δ_a is a function of the applied load gives

$$\Delta_a = \Delta_{tp} - \frac{\Delta_{co}}{L_g} L = \left(\frac{\sigma}{E_{tp}} - \frac{\sigma}{E_c} \right) L \tag{2}$$

where L is the distance between the hardened rigid platens; σ is the applied stress; and E_{tp} and E_c are the initial tangent moduli of the concrete based on the stress-strain curves derived from the transducer and strain gauge readings, respectively.

Equations (1) and (2) give

$$\Delta_c = \Delta_{tp} - \left(\frac{\sigma}{E_{tp}} - \frac{\sigma}{E_c} \right) L \tag{3}$$

Dividing Eq. (3) by L, the actual concrete strain ε_c at any stress level σ can be obtained as follows

$$\varepsilon_c = \varepsilon_{tp} - \left(\frac{1}{E_{tp}} - \frac{1}{E_c} \right) \sigma \tag{4}$$

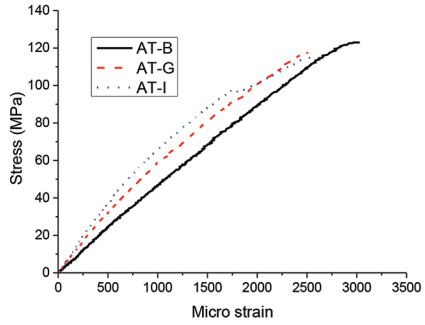

(a) ECO-UHPCC with different types of coarse aggregates

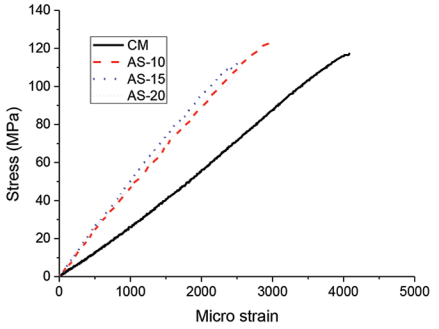

(b) ECO-UHPCC with different sizes of coarse aggregates

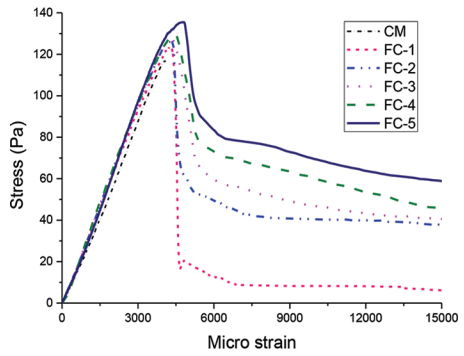

(c) ECO-UHPCC with different volume fractions of steel fiber

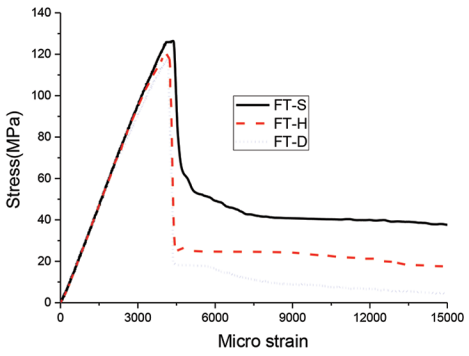

(d) ECO-UHPCC with different types of steel fiber

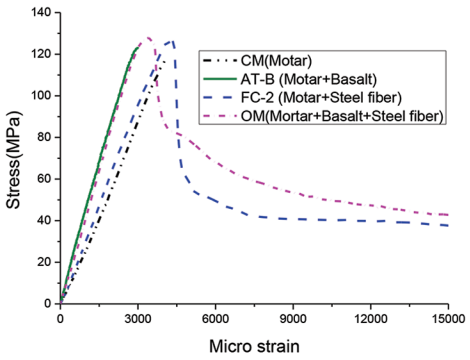

(e) ECO-UHPCC with different reinforcements

Fig. 1—Stress-strain curve of ECO-UHPCC. (Note: 1 MPa = 0.145 ksi.)

where ε_{tp} is the corresponding strain measured by transducers placed between the plates.

On the basis of the aforementioned correction method, the real complete stress-strain curve of ECO-UHPCC specimens can be obtained. According to ASTM C469,[29] the elastic modulus E_c and Poisson coefficient ν are calculated using Eq. (5) and (6), respectively.

$$E_c = \frac{S_2 - S_1}{\varepsilon_2 - 0.000050} \tag{5}$$

$$\nu = \frac{\varepsilon_{t2} - \varepsilon_{t1}}{\varepsilon_2 - 0.000050} \tag{6}$$

where S_2 is the stress corresponding to 40% of the peak stress; S_1 is the stress corresponding to a longitudinal strain of 0.00005; ε_2 is the longitudinal strain at the stress level S_2; and ε_{t2} and ε_{t1} are the transverse strains at midheight of the specimen produced by stresses S_2 and S_1, respectively.

RESULTS AND DISCUSSION

Complete stress-strain curve and failure mode

Uniaxial compressive stress-strain curves of the ECO-UHPCC with steel fiber or coarse aggregate are displayed in Fig. 1. Overall, the stress-strain curves consist of an ascending part and a descending part. However, there is no descending part of those ECO-UHPCC without steel fiber (CM, AT-series, and AS-series). As mentioned previously, although the special compressive test machine with high stiffness was used and the strain control facility was adopted in this study, the ECO-UHPCC without steel fiber showed brittle failure, and the descending part of the stress-stain curve was hard to obtain.

During the compressive test, the ECO-UHPCC specimens without steel fiber behaved elastically until peak strength

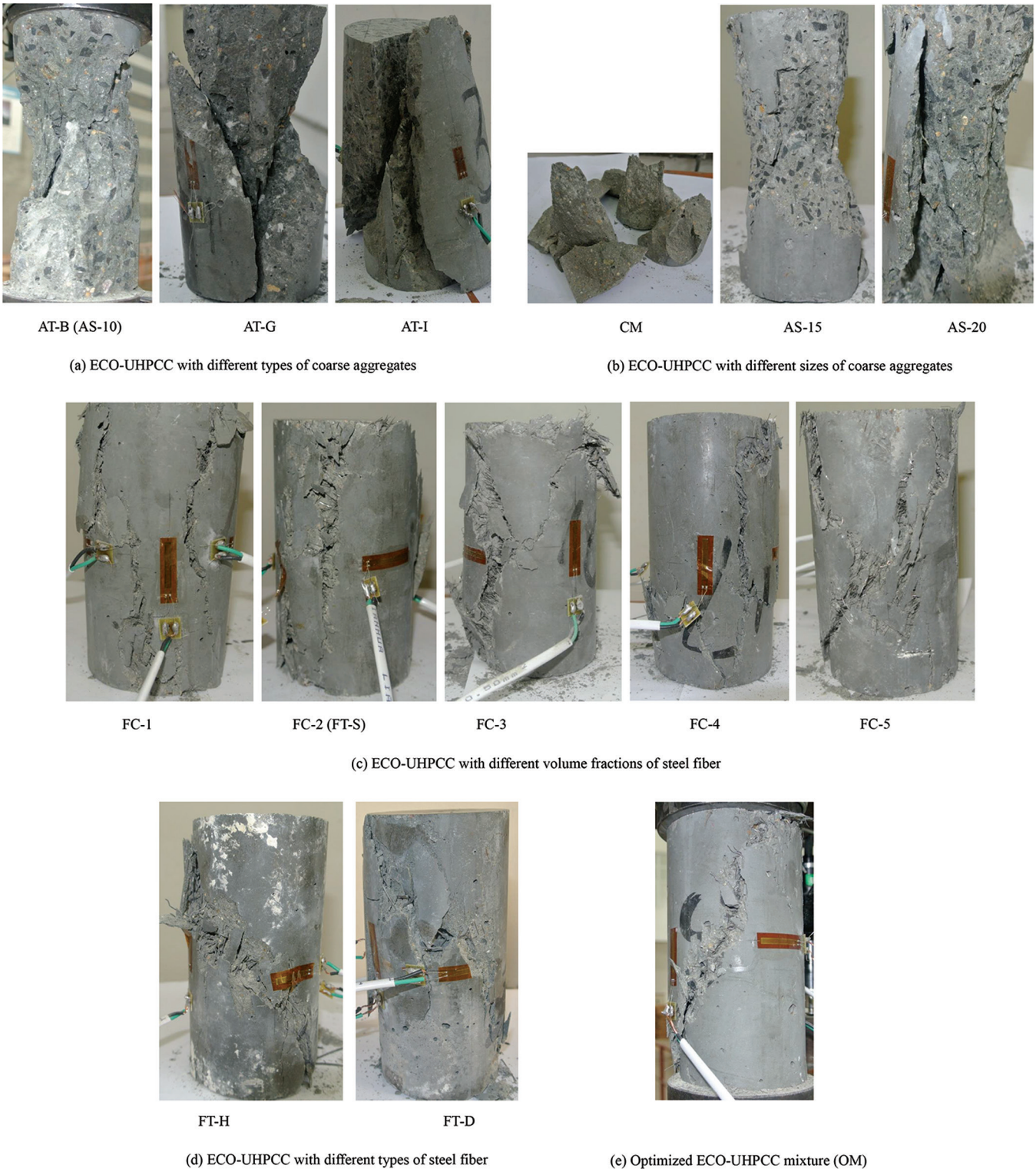

Fig. 2—Typical failure modes of cylinder specimens under compression.

and then followed with a sudden failure. With the formation of the first crack when lateral deformation exceeded its tensile capacity, the ECO-UHPCC specimens lost their total strength and failed in an abrupt, explosive manner. In contrast, ECO-UHPCC specimens with steel fiber behave elastically up to approximately 90 to 95% of their compressive strength, followed by strain hardening behavior up to peak strength. Following the peak strength, a progressive strain softening occurs in which the presence of fiber governs the softening stage.

Figure 2 shows the failure modes of the specimens. In the case of unreinforced ECO-UHPCC (CM, AT-series, and AS-series), the specimens exhibited brittle failure under uniaxial compression. The specimen showed either a cone or a cone-split failure mode, just as shown in Fig. 2(a) and Fig. 2(b). By contrast, steel fiber-reinforced ECO-UHPCC (OM, FC-series, and FT-series) showed a ductile failure mode. Beyond the peak load, as the cracks extended, the bridging effect of fibers were activated and provided lateral constraint to the specimen. The cracks along the specimen

were controlled. Instead of vertical splitting, the specimen showed a cone-shear or shear failure mode, as shown in Fig. 2(c), Fig. 2(d), and Fig. 2(e). Steel fibers prevented the microcracks from joining, and thus arrested the sudden loss of strength.[31]

Compressive strength

The full stress-strain curve of ECO-UHPCC with different types of coarse aggregate is shown in Fig. 1(a). It clearly can be seen that coarse aggregate type has a significant influence on compressive strength of ECO-UHPCC. The compressive strength of AT-B, AT-G, AT-I are 123, 118, and 115 MPa (17.835, 17.11, and 16.676 ksi), respectively. Obviously, the ECO-UHPCC with basalt coarse aggregate (AT-B) shows the highest compressive strength. It means that the basalt aggregate has a more noticeable enhancement on mechanical properties than granite and iron ore coarse aggregate. This phenomenon is different from the normal-strength concrete. For normal-strength concrete, the effect of coarse aggregate type on compressive strength is not significant.[32] It is well known that concrete is a composite, and its properties depend on the properties of the component phases (paste matrix and aggregates) and the interfacial transition zone (ITZ) between them. The compressive strength of normal-strength concrete paste matrix is low and the ITZ is weak.[33] The cracks exist in ITZ to a considerable extent before the concrete was subjected to any external load. Under loading, these small or microscopic cracks extend and interconnect until, at ultimate load, the entire internal structure is completely disrupted.[32] The aggregate had, in comparison with concrete, relatively high strength and its potential strength was not fully used. Therefore, the type of the coarse aggregate did not have an obvious effect on the compressive strength of normal-strength concrete. However, in ECO-UHPCC, the strength of the paste matrix and ITZ are vastly improved because of the very low water-binder ratio (0.16) and the use of the mineral admixture including silica fume, fly ash, and slag. With the development of loading, the cracks may extend through the aggregate, which make use of the full strength potential of the coarse aggregate particles. The coarse aggregates act as crack arrestors in ECO-UHPCC. The coarse aggregate type influences the mechanical properties of ECO-UHPCC. The stronger of coarse aggregate, the higher the ECO-UHPCC compressive strength. Therefore, the compressive strength of ECO-UHPCC with basalt coarse aggregate (AT-B) is higher than the ECO-UHPCC with granite coarse aggregate (AT-G). Aitcin and Mehta[34] also pointed out that in a high-strength concrete, the hardened cement paste and the transition zone are no longer strength limiting. The mineralogy and the strength of coarse aggregates may control the ultimate strength of concrete. Although the strength of iron coarse aggregate is higher than the basalt, the compressive strength of AT-I is lower than the AT-B. This because the strength of iron coarse aggregate (203 MPa [29.44 ksi]) is much higher than the ECO-UHPCC mortar matrix (111 MPa [16.10 ksi]). Under load, this may cause stress concentration and initiate more microcracks, resulting in a decrease in compressive strength.

Figure 1(b) presents the stress-strain curve of ECO-UHPCC with different maximum sizes of coarse aggregate. The compressive strength of CM, AS-10, AS-15, and AS-20 are 111, 123, 115, and 110 MPa (16.10, 17.84, 16.68, and 15.95 ksi), respectively. The compressive strength of ECO-UHPCC with basalt coarse aggregate (AS-10 and AS-15) is higher than that of the control mixture (CM). This phenomenon may differ from the concept of reactive powder concrete (RPC). It is well known that the coarse aggregate must be eliminated in fabrication of RPC for enhancement of homogeneity.[6] However, the tests data in this study proved that the proper maximum size of coarse aggregate beneficial for the compressive strength of ECO-UHPCC. The compressive strength decreased when the maximum size of coarse aggregate was 20 mm (0.788 in.). This phenomenon agrees with the results of self-consolidating concrete conducted by Khaleel et al.[35] This is due to smaller maximum size of coarse aggregate that has the larger surface area, which results in a higher bonding strength in the transition zone around aggregate particles when the specimen is under loading. Additionally, the increase in strength with smaller diameter may also be attributed to a change in the stress repartition inside the specimen. Each aggregate, which acts as a rather rigid inclusion inside a deformable matrix, will tend to restrain the contraction of the matrix under compressive load. Consequently, it will lead to a development of a locally nonhomogenous state of stresses around each inclusion, which depends on the aggregate diameter.[36]

From the previous discussion, it clearly can be seen that the proper coarse aggregate is helpful for fabricating of the ECO-UHPCC. The basalt coarse aggregate that exhibits a good bond, and similar strength to the surrounding ECO-UHPCC mortar matrix, and proper maximum size (10 mm [0.394 in.]), shows the best enhancement on ECO-UHPCC compressive strength.

The compressive stress-strain curve of ECO-UHPCC with different volume fractions of steel fiber is shown in Fig. 1(c). It clearly can be seen in Fig. 1(c) that the higher amount of fiber provided an improvement of the compressive strength. The highest compressive strength was found to be 138.8 MPa (20.13 ksi) for the specimen with V_f = 5% (FC-5), and this is 15.6%, 9.4%, 7.1%, 6.2%, and 4.1% higher than those of the specimens with V_f = 0 (CM), V_f = 1% (FC-1), V_f = 2% (FC-2), V_f = 3% (FC-3), and V_f = 4% (FC-4), respectively. This can be attributed to the effect of the fiber bridging mechanism. Steel fibers, mainly the ones disposed at a perpendicular direction with respect to the longitudinal cylinder axis, bridge longitudinal cracks and the eventual major inclined crack emerging when the peak load is reached. These additional resisting mechanisms oppose to damage propagation and delay the after-peak loss of load-carrying capacity.

To combine the effect of both the volume fraction of steel fiber and their aspect ratio, the reinforcing index ($RI = V_f L_f/\phi_f$) can be used as the fiber-reinforcing parameter for a given type steel fiber. V_f is the fiber content in volume fraction, L_f is the fiber length (mm), and ϕ_f is fiber diameter (mm). As shown in Fig. 3, the relationship between RI and compressive strength is linear. Based on the regression analysis of the test data, empirical models were developed for predicting the

Table 2—Mechanical properties of ECO-UHPCC

Mixture No.	Compressive strength, MPa	Elastic modulus, GPa	Poisson's ratio	Peak strain	Ultimate strain	Toughness ratio	Toughness index
CM	117.1	27.4	0.15	0.004079	0.004302	0.14	1.00
AS-10	123.0	46.9	0.23	0.003018	0.003065	0.11	0.87
AS-15	114.6	47.2	0.26	0.002549	0.002555	0.09	0.66
AS-20	110.0	46.9	0.27	0.002603	0.002603	0.09	0.65
AT-B	123.0	46.9	0.23	0.003018	0.003065	0.11	0.87
AT-G	118.0	59.0	0.25	0.002470	0.002509	0.09	0.70
AT-I	115.0	72.8	0.26	0.002612	0.002673	0.11	0.81
FC-1	123.7	31.0	0.17	0.004290	0.015000*	0.25	1.96
FC-2	126.4	31.8	0.15	0.004370	0.015000*	0.40	3.20
FC-3	127.4	31.5	0.15	0.004373	0.015000*	0.45	3.56
FC-4	130.0	32.7	0.17	0.004442	0.015000*	0.50	4.06
FC-5	135.4	30.6	0.16	0.004824	0.015000*	0.54	4.57
FT-S	126.4	31.8	0.15	0.004370	0.015000*	0.40	3.20
FT-H	121.4	31.7	0.16	0.004072	0.015000*	0.29	2.20
FT-D	117.8	31.2	0.17	0.004147	0.015000*	0.22	1.59
OM	128.4	46.2	0.26	0.003431	0.015000*	0.53	4.27

*Toughness of ECO-UHPCC specimens were computed up to strain of 0.015, although specimens still had significant resistance left.

Notes: 1 MPa = 0.145 ksi; 1 GPa = 145 ksi.

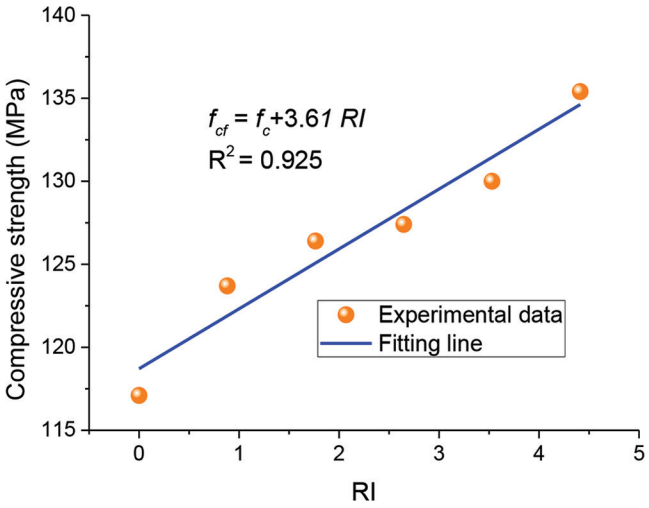

Fig. 3—Effect of RI on compressive strength. (Note: 1 MPa = 0.145 ksi.)

strength properties of steel fiber-reinforced ECO-UHPCC. The general form of the proposed strength prediction model is given by Eq. (7).

$$f_{cf} = f_c + 3.61\text{RI} \quad (7)$$

The compressive stress-strain curve of ECO-UHPCC with different types of steel fiber is shown in Fig. 1(d). The highest compressive strength is 126.4 MPa (18.33 ksi) for the specimen with micro-straight smooth steel fiber (FT-S), and this is 4.1% and 7.3% higher than those of the specimens with hooked-end (FT-H) and dumbbell steel fiber (FT-D), respectively. This phenomenon may be attributed to the fact that the peak stress is associated with adhesive bond between steel fiber and the ECO-UHPCC matrix. Although the fiber aspect ratio is the same, the diameter of micro-straight-smooth steel fiber is much smaller than the hooked-end and dumbbell steel fiber. Therefore, the contact surface area of micro-straight-smooth steel fiber is larger than that of the other two types of steel fiber.

The complete stress-strain curve of the OM mixture is shown in Fig. 1(e). As shown in Table 2, the compressive strength of OM is 128.6 MPa (18.65 ksi). This is higher than FC of 126.4 MPa (18.33 ksi). It means that the addition of coarse aggregate has the positive effect on mechanical properties of ECO-UHPCC.

Elastic modulus

The elastic modulus of ECO-UHPCC with different coarse aggregate is summarized in Table 2. As shown in Table 2, the elastic modulus of CM, OM, AS-10, AS-15, and AS-20 are 27.4, 46.2, 46.9, 47.2, and 46.9 GPa (3973.89, 6700.51, 6802.03, 6845.54, and 6802.03 ksi), respectively. Figure 1(a) also shows that the slope of the stress-strain curve of ECO-UHPCC with basalt coarse aggregate (OM, AS-10, AS-15, AS-20) is much steeper than the ECO-UHPCC without coarse aggregate (CM). It means that the addition of coarse aggregate can significantly improve the elastic modulus of ECO-UHPCC. The greater deformability observed in ECO-UHPCC without coarse aggregate may reside in the much greater paste content typically present in ECO-UHPCC mixtures than that with coarse aggregate. Because aggregates are much less deformable than hardened paste, in a hardened composition with higher paste contents, the deformability is obviously higher. Therefore, coarse aggregate is more rigid than the cement paste and will deform less under the same applied stress. However, the stress-strain curve slope of the AS-10, AS-15, and AS-20 in

Fig. 1(a) are very similar, which indicates that coarse aggregate size has little influence on the elastic modulus.

Figure 1(b) shows that the ascending part of the AT-I stress-strain curve almost overlaps those of AT-B and AT-G. As shown in Table 2, the elastic modulus of ECO-UHPCC with iron, basalt, and granite are 72.8 46.9, and 59.0 GPa (10,558.38, 6802.03, and 8556.93 ksi), respectively. This indicates that coarse aggregate type has a significant influence on elastic modulus of ECO-UHPCC. This influence was attributed to the highly dense paste structure and paste-aggregate bond, which cause the concrete to behave like a composite material.[37] Therefore, aggregate characteristics could be important in determining the elastic properties of ECO-UHPCC. The more rigid of the coarse aggregate in an ECO-UHPCC mixture, the higher elastic modulus would be. The importance of coarse aggregate quality on elastic properties of concrete was also pointed by Baalbaki et al.[38] and Beshr et al.,[37] who studied high-performance concrete and high-strength concrete, respectively.

The elastic modulus of ECO-UHPCC with different volume fraction of steel fiber is shown in Table 2. The elastic modulus of FC-1, FC-2, FC-3, FC-4, and FC-5 are 31.0, 31.8, 31.5, 32.7, and 30.6 GPa (4496.01, 4612.04, 4568.53, 4742.57, and 4438.00 ksi), respectively. This indicates that the volume fraction of steel fiber has little influence on the elastic modulus of ECO-UHPCC. This situation agrees with the study conducted by Yu-Chen et al.[39] They reported that little correlation was found between the modulus of elasticity and the reinforcing index, as expected.[39] This situation may be caused by the fact that steel fiber fraction employed in this investigation is very low ($V_f \leq 5\%$); the value of the modulus of elasticity was hardly affected. Figure 1(d) shows that the different type of steel fiber also has little influence on the elastic modulus of ECO-UHPCC. This because the steel fiber volume fractions of the three batches are the same.

Poisson's ratio

The Poisson's ratios of ECO-UHPCC are shown in Table 2. As shown in Table 2, the Poisson's ratio ranges from 0.15 to 0.27. These data agree with that reported by Perenchio and Klieger.[40] They reported values for Poisson's ratio of normalweight high-strength concrete with compressive strengths ranging from 55 to 80 MPa (7.98 to 11.60 ksi) to be between 0.20 and 0.28. However, Mehta[41] pointed out that the values of concrete Poisson's ratio generally vary between 0.15 and 0.20.

The Poisson's ratio of ECO-UHPCC with coarse aggregate (OM, AT-series, AS-series) ranges from 0.23 to 0.27. This is much higher than those ECO-UHPCC without coarse aggregate (CM, FC-series, FT-series) whose Poisson's ratio ranges from 0.15 to 0.17. Metha[42] pointed out that the Poisson's ratio does not appear to be in a consistent relationship with concrete characteristics such as water-cement ratio (w/c), curing age, and aggregate gradation. Poisson's ratio is generally lower in high-strength concrete, and higher for saturated concrete and for dynamically loaded concrete. However, there is a significant relationship between coarse aggregate and ECO-UHPCC Poisson's ratio from the data of this study. The addition of coarse aggregate results in a higher Poisson's ratio of concrete.

In fact, the addition of steel fiber did not show obvious influence on the Poisson's ratio of ECO-UHPCC. This phenomenon is in good agreement with the results given by Thomas et al.[42] They reported that the variation in the Poisson's ratio of the concrete due to the addition of steel fibers was marginal. They explained that Poisson's ratio of concrete is computed based on the observations at initial stages of loading, where the fibers do not play a significant role in the load sustenance.

Toughness

The deformation capacity and energy dissipation capacity of ECO-UHPCC were also systematically investigated in this study. Toughness ratio (TR) and toughness index (TI), defined as Eq. (8) and Eq. (9), respectively,[39] are used to quantify the toughness of different ECO-UHPCC.

$$\mathrm{TR} = \frac{ED}{0.015 f'_{cf}} \tag{8}$$

$$\mathrm{TI} = \frac{ED}{EDc} \tag{9}$$

where ED is the energy absorption capacity of ECO-UHPCC or the area under the stress-strain curve; f'_{cf} is the peak compressive stress of ECO-UHPCC. EDc is energy absorption capacity of the control specimen. Both ED and EDc are defined up to a strain of 0.015, though the specimens still had significant resistance left. The peak strain (the strain at the peak compressive stress), ultimate strain, toughness ratio (TR), and toughness index (TI) of ECO-UHPCC are summarized in Table 2.

As shown in Table 2 and Fig. 1, the highest peak strain was found to be 0.004824 for the specimen with $V_f = 5\%$ (FC-5), and this is 18.3%, 12.4%, 10.3%, 10.3%, and 8.5% higher than those of the specimens with $V_f = 0$ (CM), $V_f = 1\%$ (FC-1), $V_f = 2\%$ (FC-2), $V_f = 3\%$ (FC-3), and $V_f = 4\%$ (FC-4), respectively. However, the peak strain of ECO-UHPCC without steel fiber are much smaller than that with steel fiber. The peak strain of AT-series and AS-series range from 0.002500 to 0.003000. As discussed in the "Complete stress-strain curve and failure mode" section, the specimen of ECO-UHPCC without steel fiber showed brittle failure during the compressive tests and there was no descending part of the stress-train curve. The addition of steel fiber significantly enhanced the deformation capacity of the ECO-UHPCC.

The toughness index of AT-series and AS-series range from 0.65 to 0.87, which is less than 1.0 of the control mixture. This means that the energy dissipation capacity of the ECO-UHPCC with coarse aggregate is weaker than that of the control mixture. Additionally, the maximum size of coarse aggregate influences the toughness index. The larger the coarse aggregate, the smaller the toughness index. This may be attributed to the fact that the addition of coarse aggregate constrains the deformation ability of the ECO-UHPCC, as discussed previously.

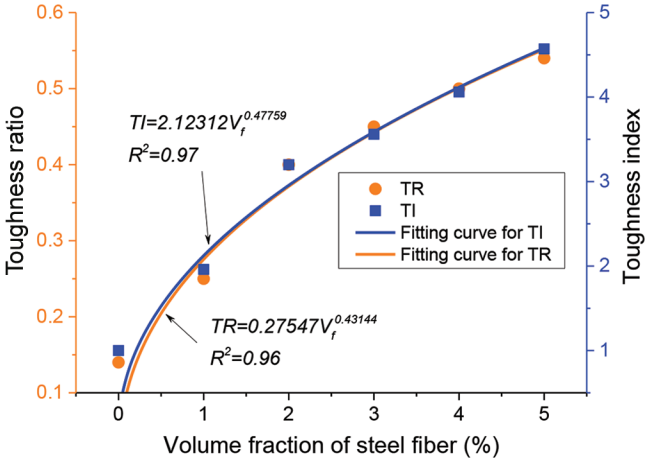

Fig. 4—Relationship between TR, TI, and volume fraction of steel fiber.

The toughness index values of OM, FC-series, and FT-series range from 1.59 to 4.57, which is much higher than that of the control mixture. ECO-UHPCC with steel fiber shows excellent energy dissipation capacity. ECO-UHPCC reinforced with higher contents of fibers show a more extended softening branch. Therefore, the area under stress-strain curve of ECO-UHPCC with more steel fiber were much larger than lesser one. The TI of OM is 4.27, which is higher than the FC-4 of 4.06. The addition of coarse aggregate is helpful for the toughness of steel fiber-reinforced ECO-UHPCC. On the basis of tests data of the FC-series and CM, the relationship between TR, RI, and volume fraction of steel fiber regressed as Eq. (10), Eq. (11), and the fitting curve are shown in Fig. 4.

$$\mathrm{TR} = 0.2754V_f^{0.43144} \quad (R^2 = 0.96) \tag{10}$$

$$\mathrm{TI} = 2.12312V_f^{0.47759} \quad (R^2 = 0.97) \tag{11}$$

It clearly can be seen from Fig. 4 that the relationship between TR, TI, and volume fraction of steel fibers are both power functions. The fitting curve of toughness ratio and toughness index are very similar to each other.

ANALYTICAL MODELS OF COMPRESSIVE STRESS-STRAIN RELATIONSHIP

The compressive stress-strain relationship of ECO-UHPCC is important in the analysis and design of structural members. In the last few decades, few analytical models have been proposed for predicting the behavior of ECO-UHPCC under uniaxial compression. Accordingly, the model proposed by Graybeal[21] for the ultra-high-performance fiber-reinforced concrete (UHPFRC) is shown as follows

$$\sigma = \varepsilon E(1 - \alpha) \tag{12}$$

Equation (12) shows the actual stress σ and strain ε values are related by the modulus of elasticity E and a reduction factor α. α was defined as the decrease in the actual stress from the linear elastic stress, which is shown as Eq. (13), where a and b are the fitting parameters.

$$\alpha = ae^{\frac{\varepsilon E}{bf_c'}} - a \tag{13}$$

This model showed good agreement with the experimental results of UHPFRC in Graybeal's[21] research. Zhou et al.[43] also used this model to predict the ascending part of engineering cementitious composites (ECCs). However, as the compressive strength of UHPFRC was too high, the descending part of the stress-strain curve could not be obtained in that study.

In the present study, the analytical expression of the stress-strain law suggested by CEB-FIP Model Code[44] was introduced as the basic model equation to predict the ascending part of the curves. The shape of the equation has good correlation with experimental results in this study. The expression is

$$\frac{\sigma}{f_c'} = \frac{A\left(\frac{\varepsilon}{\varepsilon_0}\right) - \left(\frac{\varepsilon}{\varepsilon_0}\right)^2}{1 + (A-2)\left(\frac{\varepsilon}{\varepsilon_0}\right)} \quad (\varepsilon \le \varepsilon_0) \tag{14}$$

where σ and ε are the actual stress and actual strain value, respectively; f_c' and ε_0 are the peak stress (compressive strength) and peak strain, respectively; and A is a parameter that controls the ascending branch of the curve.

The stress-strain curve represented by Eq. (14) has a defect, which underpredicts the decline of the stress-strain curve. Therefore, a new model must be proposed to satisfy descending part of the curves. The following conditions should be considered to represent the complete descending branch of the stress-strain curve

1. $\sigma(1)/f_c' = 1$, the stress equals the peak stress for $\varepsilon_0 = \varepsilon(1) = 1$;
2. $\frac{d}{d\varepsilon}\frac{\sigma(\varepsilon)}{f_c'} = 0$, the descending curve has a zero tangent at the peak stress; and
3. $\lim_{\varepsilon\to\infty}\frac{\sigma(\varepsilon)}{f_c'} = 0$

Assimilating all these conditions, the formulation of the softening branch of the stress-strain curve was proposed

$$\frac{\sigma}{f_c'} = \frac{1}{B \times \left(\frac{\varepsilon}{\varepsilon_0}\right)^C + 1 - B} \quad (\varepsilon \ge \varepsilon_0) \tag{15}$$

where B and C are parameters that control the descending branch of the curve. Equations (14) and (15) can be used to generate the complete stress-strain curve for different A-, B-, and C-values in normalized manner. Those values are summarized in Table 3. In this table, the symbol "—" means that the descending branch is not available for the ECO-UHPCC without steel fiber. The ascending part of the stress-strain curve is effected by the A-value. As the A-value increases, the slope of the curve increases, meaning that the elastic modulus of the ECO-UHPCC increases. There-

Table 3—Values of parameters *A*, *B*, and *C* for different ECO-UHPCC

Mixture No.		Ascending part	Descending part		
		A	B	C	R^2
	CM	1.00385	—	—	0.99721
Fiber content	FC-1	1.07278	19.16287	1.11616	0.92502
	FC-2	1.11079	46001.91592	9.3868×10^{-5}	0.73140
	FC-3	1.07738	9043.41488	2.71588×10^{-5}	0.99559
	FC-4	1.10733	9292.72487	1.95629×10^{-5}	0.96709
	FC-5	1.14915	7552.30288	1.93417×10^{-4}	0.84696
Fiber type	FT-H	1.05611	167630.7218	5.8062×10^{-5}	0.81959
	FT-D	1.07968	71161.1575	2.62591×10^{-4}	0.98097
Aggregate type	AT-B	1.12343	—	—	0.99946
	AT-G	1.22873	—	—	0.99405
	AT-I	1.71888	—	—	0.99690
Aggregate size	AS-10	1.14139	—	—	0.99966
	AS-15	1.09602	—	—	0.99857
	AS-20	1.12447	—	—	0.99777
	OM	1.17989	3479.43588	4.2996×10^{-4}	0.96784

fore, the *A*-value is related to the elastic modulus of the ECO-UHPCC. The descending part of the stress-strain curve is effected by the *B*- and *C*-values.

The comparison of proposed model equations with experimental results is shown in Fig. 5. Obviously, there is a good correlation between the experimentally measured stress-strain curves with the analytical curves.

CONCLUSIONS

Based on the results of this study, the following conclusions can be made:

1. An ecological ultra-high-performance cementitious composite (ECO-UHPCC) was successfully fabricated. A large amount of portland cement (≥50%) was replaced by industrial waste, including fly ash, slag, and silica fume. The cement content of ECO-UHPCC ranged from 400 to 520 kg/m^3 (24.97 to 32.46 lb/ft^3). Natural river sand and various coarse aggregates were substitutes for the costly ultra-fine quartz sand.

2. The ECO-UHPCC has an equivalent mechanical performance with UHPCC. The compressive strength and elastic modulus of ECO-UHPCC containing basalt coarse aggregate with a maximum size of 10 mm (0.394 in.) and 2% steel fiber were up to 128.4 MPa (18.62 ksi) and 46.2 GPa (6700.51 ksi), respectively.

3. A new model was developed for predicting the full stress-strain behavior of ECO-UHPCC under uniaxial compression. This model shows a good correlation between the experimental results.

AUTHOR BIOS

Zhiyong Liu *is an Associate Professor in the State Key Laboratory of Geomechanics & Deep Underground Engineering at China University of Mining and Technology, Xuzhou, China. He received his PhD in material Science from Southeast University, Nanjing, China, in 2013. His research interests include nondestructive testing, microstructure, and transport properties of cement-based materials.*

Weiwei Chen *is a Graduate Student in the Jiangsu Key Laboratory of Environmental Impact and Structural Safety in Engineering, China University of Mining and Technology. His research interests include characterization and modeling of concrete microstructure.*

Wenhua Zhang *is an Associate Professor at Nanjing Forestry University, Nanjing, China. He received his PhD in material science from Southeast University in 2012. His research interests include durability of high-performance concrete.*

Yunsheng Zhang *is a Professor in the Jiangsu Key Laboratory for Construction Materials of Southeast University. He received his PhD in structure engineering from Southeast University in 2004. His research interests include geopolymeric cement and its composites, high-performance concrete made with fly ash or slag, durability, and service life prediction of high-performance concrete.*

Henglin Lv *is a Professor at China University of Mining and Technology, where he also received his PhD in structure engineering. His research interests include durability of reinforced concrete.*

ACKNOWLEDGMENTS

The authors gratefully acknowledge the financial support of the National Natural Science Foundation of China (51778613) and the Fundamental Research Funds for the Central Universities (2015XKMS011).

REFERENCES

1. Richard, P., and Cheyrezy, M., "Composition of Reactive Powder Concretes," *Cement and Concrete Research*, V. 25, No. 7, 1995, pp. 1501-1511. doi: 10.1016/0008-8846(95)00144-2

2. Wille, K.; El-Tawil, S.; and Naaman, A. E., "Properties of Strain Hardening Ultra-High Performance Fiber Reinforced Concrete (UHP-FRC) under Direct Tensile Loading," *Cement and Concrete Composites*, V. 48, 2014, pp. 53-66. doi: 10.1016/j.cemconcomp.2013.12.015

3. Rong, Z., and Sun, W., "Experimental and Numerical Investigation on the Dynamic Tensile Behavior of Ultra-High Performance Cement-Based Composites," *Construction and Building Materials*, V. 31, 2012, pp. 168-173. doi: 10.1016/j.conbuildmat.2011.12.058

4. Zhang, W.; Zhang, Y.; and Zhang, G., "Static, Dynamic Mechanical Properties and Microstructure Characteristics of Ultra-High Performance Cementitious Composites," *Science and Engineering of Composite Materials*, V. 19, No. 3, 2012, doi: 10.1515/secm-2011-0136

5. Yang, S. L.; Millard, S. G.; Soutsos, M. N.; Barnett, S. J.; and Le, T. T., "Influence of Aggregate and Curing Regime on the Mechanical Properties of Ultra-High Performance Fibre Reinforced Concrete (UHPFRC),"

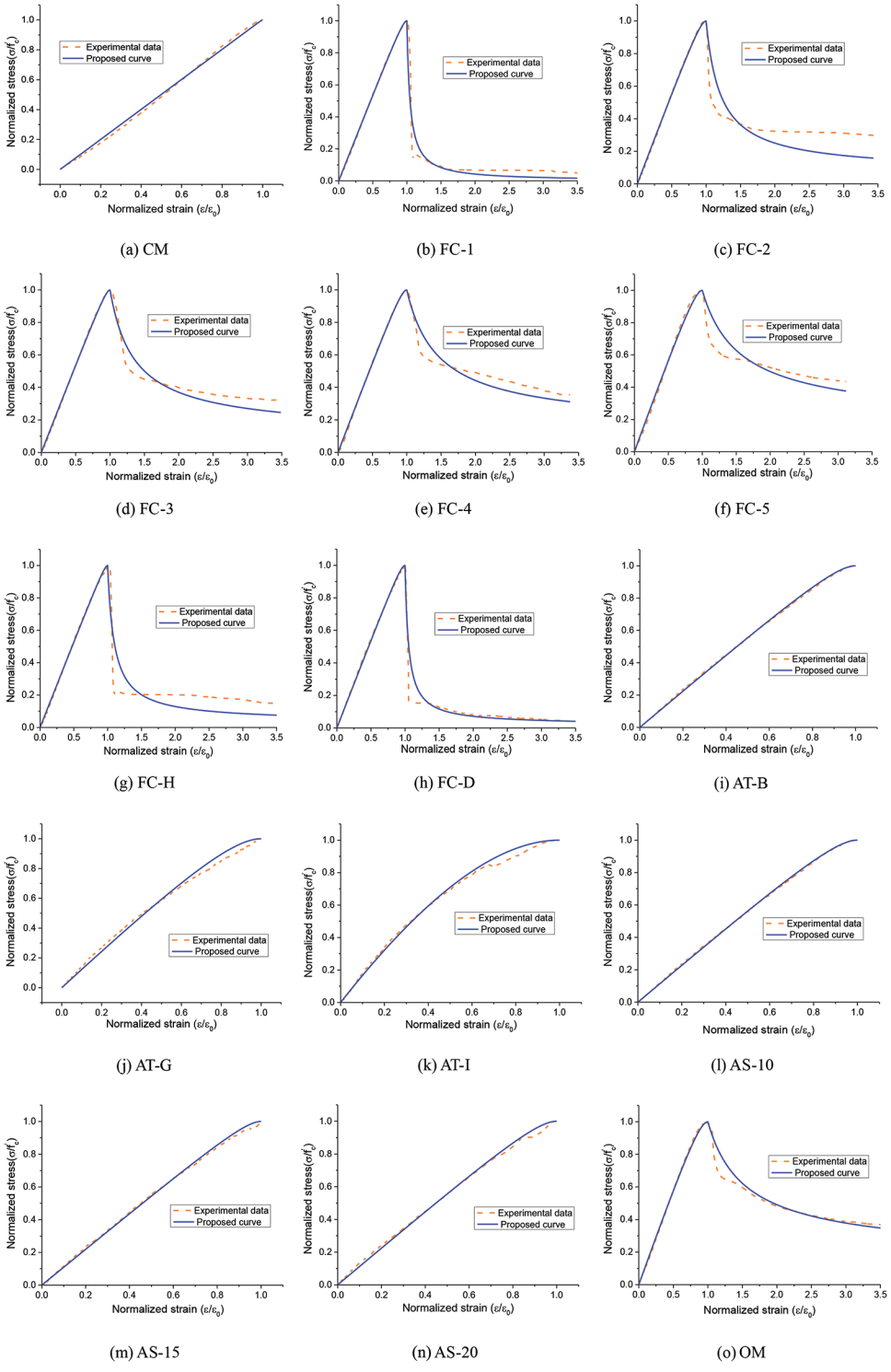

Fig. 5—Comparison of proposed model equations with experimental results.

Construction and Building Materials, V. 23, No. 6, 2009, pp. 2291-2298. doi: 10.1016/j.conbuildmat.2008.11.012

6. Zhang, W.; Zhang, Y.; and Zhang, G., "Single and Multiple Dynamic Impacts Behaviour of Ultra-High Performance Cementitious Composite," *Journal of Wuhan University of Technology – Materials*, V. 26, No. 6, 2011, pp. 1227-1234. doi: 10.1007/s11595-011-0395-x

7. Yunsheng, Z.; Wei, S.; Sifeng, L.; Chujie, J.; and Jianzhong, L., "Preparation of C200 Green Reactive Powder Concrete and its Static-Dynamic Behaviors," *Cement and Concrete Composites*, V. 30, No. 9, 2008, pp. 831-838. doi: 10.1016/j.cemconcomp.2008.06.008

8. Lima, C.; Caggiano, A.; Faella, C.; Martinelli, E.; Pepe, M.; and Realfonzo, R., "Physical Properties and Mechanical Behaviour of Concrete Made with Recycled Aggregates and Fly Ash," *Construction and Building Materials*, V. 47, 2013, pp. 547-559. doi: 10.1016/j.conbuildmat.2013.04.051

9. Yazıcı, H.; Yiğiter, H.; Karabulut, A.; and Baradan, B., "Utilization of Fly Ash and Ground Granulated Blast Furnace Slag as an Alternative Silica Source in Reactive Powder Concrete," *Fuel*, V. 87, No. 12, 2008, pp. 2401-2407. doi: 10.1016/j.fuel.2008.03.005

10. Cwirzen, A.; Penttala, V.; and Vornanen, C., "Reactive Powder Based Concretes: Mechanical Properties, Durability and Hybrid Use with OPC," *Cement and Concrete Research*, V. 38, No. 10, 2008, pp. 1217-1226. doi: 10.1016/j.cemconres.2008.03.013

11. Feylessoufi, A.; Crespin, M.; Dion, P.; Bergaya, F.; Van Damme, H.; and Richard, P., "Controlled Rate Thermal Treatment of Reactive Powder Concretes," *Advanced Cement Based Materials*, V. 6, No. 1, 1997, pp. 21-27. doi: 10.1016/S1065-7355(97)90002-X

12. Yoo, D.; Min, K.; Lee, J.; and Yoon, Y., "Shrinkage and Cracking of Restrained Ultra-High-Performance Fiber-Reinforced Concrete Slabs at

Early Age," *Construction and Building Materials*, V. 73, 2014, pp. 357-365. doi: 10.1016/j.conbuildmat.2014.09.097

13. Yoo, D.; Park, J.; Kim, S.; and Yoon, Y., "Early Age Setting, Shrinkage and Tensile Characteristics of Ultra High Performance Fiber Reinforced Concrete," *Construction and Building Materials*, V. 41, 2013, pp. 427-438. doi: 10.1016/j.conbuildmat.2012.12.015

14. Soliman, A. M., and Nehdi, M. L., "Effects of Shrinkage Reducing Admixture and Wollastonite Microfiber on Early-Age Behavior of Ultra-High Performance Concrete," *Cement and Concrete Composites*, V. 46, 2014, pp. 81-89. doi: 10.1016/j.cemconcomp.2013.11.008

15. Yoo, D.; Park, J.; Kim, S.; and Yoon, Y., "Influence of Reinforcing Bar Type on Autogenous Shrinkage Stress and Bond Behavior of Ultra High Performance Fiber Reinforced Concrete," *Cement and Concrete Composites*, V. 48, 2014, pp. 150-161. doi: 10.1016/j.cemconcomp.2013.11.014

16. Wille, K.; Naaman, A. E.; El-Tawil, S.; and Parra-Montesinos, G. J., "Ultra-High Performance Concrete and Fiber Reinforced Concrete: Achieving Strength and Ductility without Heat Curing," *Materials and Structures*, V. 45, No. 3, 2012, pp. 309-324. doi: 10.1617/s11527-011-9767-0

17. Habel, K.; Viviani, M.; Denarié, E.; and Brühwiler, E., "Development of the Mechanical Properties of an Ultra-High Performance Fiber Reinforced Concrete (UHPFRC)," *Cement and Concrete Research*, V. 36, No. 7, 2006, pp. 1362-1370. doi: 10.1016/j.cemconres.2006.03.009

18. Aldahdooh, M. A. A.; Muhamad Bunnori, N.; and Megat Johari, M. A., "Development of Green Ultra-High Performance Fiber Reinforced Concrete Containing Ultrafine Palm Oil Fuel Ash," *Construction and Building Materials*, V. 48, 2013, pp. 379-389. doi: 10.1016/j.conbuildmat.2013.07.007

19. Habel, K., and Gauvreau, P., "Response of Ultra-High Performance Fiber Reinforced Concrete (UHPFRC) to Impact and Static Loading," *Cement and Concrete Composites*, V. 30, No. 10, 2008, pp. 938-946. doi: 10.1016/j.cemconcomp.2008.09.001

20. Lai, J., and Sun, W., "Dynamic Behaviour and Visco-elastic Damage Model of Ultra-High Performance Cementitious Composite," *Cement and Concrete Research*, V. 39, No. 11, 2009, pp. 1044-1051. doi: 10.1016/j.cemconres.2009.07.012

21. Graybeal, B. A., "Compressive Behavior of Ultra-High-Performance Fiber-Reinforced Concrete," *ACI Materials Journal*, V. 104, No. 2, Mar.-Apr. 2007, pp. 146-152.

22. Zanni, H.; Cheyrezy, M.; Maret, V.; Philippot, S.; and Nieto, P., "Investigation of Hydration and Pozzolanic Reaction in Reactive Powder Concrete (RPC) Using 29Si NMR," *Cement and Concrete Research*, V. 26, No. 1, 1996, pp. 93-100. doi: 10.1016/0008-8846(95)00197-2

23. ASTM C33-03, "Standard Specification for Concrete Aggregates," ASTM International, West Conshohocken, PA, 2003, 11 pp.

24. ASTM C127-01, "Standard Test Method for Density, Relative Density (Specific Gravity), and Absorption of Coarse Aggregate," ASTM International, West Conshohocken, PA, 2001, 6 pp.

25. GB/T14685-2001, "Pebble and Crushed Stone for Building," China Standards, 1992.

26. ASTM C192/C192M-06, "Standard Practice for Making and Curing Concrete Test Specimens in the Laboratory," ASTM International, West Conshohocken, PA, 2006, 8 pp.

27. Hassan, A. M. T.; Jones, S. W.; and Mahmud, G. H., "Experimental Test Methods to Determine the Uniaxial Tensile and Compressive Behaviour of Ultra High Performance Fibre Reinforced Concrete (UHPFRC)," *Construction and Building Materials*, V. 37, 2012, pp. 874-882. doi: 10.1016/j.conbuildmat.2012.04.030

28. Mansur, M. A.; Wee, T. H.; and Chin, M. S., "Derivation of the Complete Stress-Strain Curves for Concrete in Compression," *Magazine of Concrete Research*, V. 47, No. 173, 1995, pp. 285-290. doi: 10.1680/macr.1995.47.173.285

29. ASTM C469/C469M-10, "Standard Test Method for Static Modulus of Elasticity and Poisson's Ratio of Concrete in Compression," ASTM International, West Conshohocken, PA, 2010, 5 pp.

30. ASTM C39/C39M-11, "Standard Test Method for Compressive Strength of Cylindrical Concrete Specimens," ASTM International, West Conshohocken, PA, 2011, 7 pp.

31. Kayali, O.; Haque, M. N.; and Zhu, B., "Some Characteristics of High Strength Fiber Reinforced Lightweight Aggregate Concrete," *Cement and Concrete Composites*, V. 25, No. 2, 2003, pp. 207-213. doi: 10.1016/S0958-9465(02)00016-1

32. Wu, K.; Chen, B.; Yao, W.; and Zhang, D., "Effect of Coarse Aggregate Type on Mechanical Properties of High-Performance Concrete," *Cement and Concrete Research*, V. 31, No. 10, 2001, pp. 1421-1425. doi: 10.1016/S0008-8846(01)00588-9

33. Beshr, H.; Almusallam, A. A.; and Maslehuddin, M., "Effect of Coarse Aggregate Quality on the Mechanical Properties of High Strength Concrete," *Construction and Building Materials*, V. 17, No. 2, 2003, pp. 97-103. doi: 10.1016/S0950-0618(02)00097-1

34. Aitcin, P. C., and Mehta, P. K., "Effect of Coarse Aggregate Characteristics on Mechanical Properties of High-Strength Concrete," *ACI Materials Journal*, V. 87, No. 2, Mar.-Apr. 1990, pp. 103-107.

35. Khaleel, O. R.; Al-Mishhadani, S. A.; and Abdul Razak, H., "The Effect of Coarse Aggregate on Fresh and Hardened Properties of Self-Compacting Concrete (SCC)," *Procedia Engineering*, V. 14, 2011, pp. 805-813. doi: 10.1016/j.proeng.2011.07.102

36. Szczesniak, M.; Rougelot, T.; Burlion, N.; and Shao, J. F., "Compressive Strength of Cement-Based Composites: Roles of Aggregate Diameter and Water Saturation Degree," *Cement and Concrete Composites*, V. 37, 2013, pp. 249-258. doi: 10.1016/j.cemconcomp.2012.08.001

37. Beshr, H.; Almusallam, A. A.; and Maslehuddin, M., "Effect of Coarse Aggregate Quality on the Mechanical Properties of High Strength Concrete," *Construction and Building Materials*, V. 17, No. 2, 2003, pp. 97-103. doi: 10.1016/S0950-0618(02)00097-1

38. Baalbaki, W.; Benmokrane, B.; Chaallal, O.; and Aitcin, P., "Influence of Coarse Aggregate on Elastic Properties of High-Performance Concrete," *ACI Materials Journal*, V. 88, No. 5, Sept.-Oct. 1991, pp. 499-503.

39. Ou, Y.; Tsai, M.; Liu, K.; and Chang, K., "Compressive Behavior of Steel-Fiber-Reinforced Concrete with a High Reinforcing Index," *Journal of Materials in Civil Engineering*, ASCE, V. 24, No. 2, 2012, pp. 207-215. doi: 10.1061/(ASCE)MT.1943-5533.0000372

40. Perenchio, W. F., and Klieger, P., *Some Physical Properties of High-Strength Concrete*, Portland Cement Association, Skokie, IL, 1978, 56 pp.

41. Mehta, P. K., and Monteiro, P. J., *Concrete: Microstructure, Properties, and Materials*, McGraw-Hill, New York, 2006, 93 pp.

42. Thomas, J., and Ramaswamy, A., "Mechanical Properties of Steel Fiber-Reinforced Concrete," *Journal of Materials in Civil Engineering*, ASCE, V. 19, No. 5, 2007, pp. 385-392. doi: 10.1061/(ASCE)0899-1561(2007)19:5(385)

43. Zhou, J.; Pan, J.; and Leung, C. K. Y., "Mechanical Behavior of Fiber-Reinforced Engineered Cementitious Composites in Uniaxial Compression," *Journal of Materials in Civil Engineering*, ASCE, V. 27, No. 1, 2015, 04014111, doi: 10.1061/(ASCE)MT.1943-5533.0001034

44. CEB-FIP Model Code, "Design of Concrete Structures," British Standards Institution, London, UK, 1993, 2 pp.